Zayed *et al. Stem Cell Research & Therapy* (2025) 16:154
https://doi.org/10.1186/s13287-025-04273-x

Stem Cell Research & Therapy

RESEARCH

Open Access

Biological characteristics and transcriptomic profile of adipose-derived mesenchymal stem cells isolated from prion-infected murine model

Mohammed Zayed[1,2,3†], Yong-Chan Kim[4,5†] and Byung-Hoon Jeong[1,2*]

Abstract

Background Prion diseases are characterized by accumulation of misfolded host prion proteins (PrP^{Sc}) that produce aggregates in brain tissue. Mesenchymal stem cells (MSCs) have been identified as potential therapeutic candidates for prion diseases. However, it has been demonstrated that MSCs maintained and expressed PrP^{Sc} levels following inoculation, raising concerns regarding their safe and effective use in medical applications. Prion infectivity has been reported in fat tissues, thus the response of adipose-derived MSCs (AdMSCs) to prion infection needs to be fully studied.

Methods For this study, we analyzed the properties of AdMSCs isolated from mice infected with the ME7 scrapie strain and compared them with negative controls. We investigated morphology, viability, immunophenotyping, markers of inflammation, migration activity, and neurotrophic factors. RNA sequencing (RNA-Seq) was performed to identify transcriptome profile changes.

Results AdMSCs derived from ME7-infected mice displayed immunophenotypes similar to cells from negative controls, but they were larger with lower viability ($p < 0.05$). ME7 infection caused higher expression of inflammatory mediators *CCL5*, *TNF-a*, *C3*, and *IL6* ($p < 0.05$ and $p < 0.01$) and low expression of the stem cell marker, *CXCR4* ($p < 0.05$) which was confirmed by immunofluorescence staining. The results showed decreased migration activity and wound closure ability of AdMSCs isolated from ME7-infected mice as confirmed by Transwell migration and scratch wound assays ($p < 0.05$ and $p < 0.001$), respectively. The RNA-Seq results detected 367 differentially expressed genes between AdMSCs from ME7-infected mice and those from the negative controls, and negative regulation of locomotion, extracellular matrix (ECM) organization, collagen-containing ECM, and extracellular structure organization genes were common in AdMSCs from ME7-infected mice. Transcriptomic analysis revealed that pathways enriched in AdMSCs from ME7-infected mice included those involved in the PI3K-Akt signaling pathway, cell adhesion, protein digestion and absorption, and cytokine–cytokine receptor interactions. Interestingly, genes related to the regulation of iron storage, such as *Hp* and *hepcidin*, were upregulated in AdMSCs isolated from ME7-infected mice.

Conclusions Based on these data, therapeutic strategies for AdMSCs in prion disease should be further investigated.

Keywords Stem cells, Neurodegenerative disease, Prion disease, RNA-Seq, Characterization, Allogenic, Adipose tissue, Transcriptomic analysis

†Mohammed Zayed and Yong-Chan Kim have contributed equally to this work.

*Correspondence:
Byung-Hoon Jeong
bhjeong@jbnu.ac.kr
Full list of author information is available at the end of the article

Background

Prion diseases are fatal neurodegenerative disorders caused by a conformational change of cellular prion protein (PrP^{C}) to an abnormal isoform (PrP^{Sc}) [1, 2]. PrP^{Sc} is partially resistant to protease digestion and tends to form aggregations [1]. In addition to histopathological signs such as widespread spongiform encephalopathy and deposition of aggregated PrP^{C}, PrP^{Sc} causes neurotoxicity [3, 4], resulting in extensive and progressive brain degeneration [5]. Although the accumulation of pathological isoforms principally occurs in brain tissues, it also is observed in the kidney, liver, lung, and bone marrow [6–8]. Race et al. identified prion infectivity in fat tissues collected from scrapie-infected mice [9]. Therefore, such tissues infected with prions could present an unrecognized risk for infection spread to humans or domestic animals.

Mesenchymal stem cells (MSCs) are fibroblast-like cells characterized by self-renewal and differentiation into mesodermal tissues (osteoblasts, adipocytes, and chondrocytes) [10–12]. Due to their capacity to migrate to sites of neuroinflammation and to secrete cytokines, growth factors, and neuromodulators, MSCs are attractive candidates for treating neurological disorders, such as prion diseases [13–15]. Adipose tissue can be easily accessed and collected regularly under local anesthesia with minimal discomfort for the patient, and it also contains a higher concentration of MSCs compared to bone marrow [16]. Adipose-derived MSCs (AdMSCs) instantly attach to plastic culture flasks, proliferate in vitro, and differentiate into several cell lineages with potential tissue regeneration similar to other MSCs [17, 18]. AdMSCs also secrete neuroprotective factors to prevent neuronal damage [19], and AdMSC transplantation has become a widely used therapeutic modality for various diseases [17]. Recently, intranasal administration of AdMSCs was found to reduce vacuolization across brain tissues, decrease the number of astrocytes, and downregulate inflammasome signaling genes in a mouse-adapted prion model [20]. In addition, AdMSCs secretome has demonstrated the potential to attenuate PrP^{C} peptide (106–126)-induced oxidative stress [21]. Therefore, AdMSCs could play a promising role as a cell-based therapy for prion diseases.

A major challenge in MSC-based prion therapies for prion diseases is the potential infectivity of MSCs isolated from bone marrow or adipose tissue, as validated by tissue-derived homogenate-inoculated mice [9, 22]. Bone marrow-derived MSCs (BM-MSCs) expressed PrP^{Sc} [23] and sustained PrP^{Sc} level post-inoculation [24]. Furthermore, after in vitro exposure to a prion strain, BM-MSCs remained persistently infected, generating PrP^{Sc} during multiple passages [25]. Also, the detection of prion infectivity in MSCs from individuals affected by prion diseases has been reported. For example, the presence of PrP^{Sc} in BM-MSCs isolated from Creutzfeldt-Jakob disease (CJD) patients has been reported [26]. This could raise concerns about the safe and effective implementation of medical practices and necessitates care when applying stem cells from individuals infected with prions in clinical settings.

Autologous and allogeneic MSCs are of interest for cell therapy to treat neurodegenerative diseases [27]. In the body, transplanted MSCs interact with their microenvironment either physiologically or pathologically. These cells can change their distinct biological activity in a newly developed tissue microenvironment as a result of detrimental environmental stimuli [28]. Compared with allogeneic MSCs, autologous MSCs from patients who require cell-based therapy could be an ideal source [29, 30], despite their potential to carry systemic diseases. However, the therapeutic capacity of autologous stem cells is impaired in disease conditions [31, 32]. Pathological microenvironments adversely affect MSCs, impacting their growth, proliferation, migration, apoptosis, and differentiation [33]. These effects are also influenced by both the type and severity of the disease. Still, characterization of MSCs from a disease state is rare. RNA sequencing (RNA-Seq) offers insight into a cell's transcriptome and can allow researchers to identify genes implicated in a biological process of interest [34]. To the best of our knowledge, the transcriptome analysis of AdMSCs in response to prion infection is incomplete. In this work, we analyzed the properties of AdMSCs isolated from mice inoculated with the ME7 scrapie strain (an experimental model of prion disease). We evaluated how prion infection affected the characteristics of the MSCs and performed a transcriptome analysis.

Materials and methods

Experimental prion disease model

C57BL/6 J mice (6 weeks old) were purchased from Nara Biotech (Pyeongtaek, Gyeonggi, Korea).

The animal experiments were performed in accordance with protocols approved by the Institutional Animal Care and Use Committee at Jeonbuk National University (JBNU 2020–080). The work has been reported in line with the ARRIVE guidelines 2.0. An animal model of prion disease based on intraperitoneal injection of the ME7 scrapie strain into C57BL/6 mice was previously reported [35]. Before intraperitoneal injection, all mice were anesthetized with 2% isoflurane (Hana Pharm Co., Ltd; Seoul, South Korea) in an induction chamber. Briefly, the mice (n = 6) were inoculated via intraperitoneal injection with 100 µl of 1% (w/v) brain homogenate prepared from terminally ill ME7-infected mice. For the negative

control, mice (n = 6) were inoculated via intraperitoneal injection with 100 µl of phosphate-buffered saline (PBS, Gibco, NY, USA). After five months of inoculation, the mice were deeply anesthetized with isoflurane and euthanized by cervical dislocation to minimize distress.

Western blotting

To detect total PrP and glial fibrillary acidic protein (GFAP), whole brain tissues from the ME7-infected and negative control mice (n = 3/group) were separately homogenized with a 10% volume of RIPA lysis buffer (Thermo Fisher Scientific, Waltham, MA, USA) containing a protease inhibitor cocktail (Roche, Munich, Germany). To detect PrP^{Sc}, 50 µg/mL proteinase K (Sigma-Aldrich, MO, USA) was added to the brain tissue homogenates for 1 h at 37 °C. The samples were separated via sodium dodecyl sulfate–polyacrylamide gel electrophoresis on 12% gels. The gels were then electroblotted onto polyvinylidene difluoride membranes (Amersham, Little Chalfont, UK) using an electrophoretic transfer system (Bio-Rad, Hércules, USA) at 100 V for 1.5 h. Each membrane was washed and then blocked in 5% skim milk for 2 h before incubation with the primary antibodies, SAF84 (1:200, Cat#: A03208, Bertin, Montigny le Bretonneux-France) or GFAP (1:200, Cat#: sc-33673, Santa Cruz Biotechnology, Dallas, Texas, USA). Then, each membrane was washed and incubated with anti-mouse secondary antibodies (Sigma-Aldrich). Protein levels were normalized to that of Purified Mouse Anti-Hsp90 (BD Transduction Laboratory). Immunoreactive bands were visualized with a Pierce ECL kit (Thermo Fisher Scientific).

Isolation and culturing of AdMSCs

Mice were euthanized following isoflurane anesthesia and cervical dislocation, and adipose tissue samples from the negative control (n = 3) and ME7-infected mice (n = 3) were collected and washed with PBS for isolation of AdMSCs as we previously demonstrated [21]. In brief, the tissues were then chopped into small pieces and shaken for 45 min at 37 °C with 0.1% type I collagenase (Sigma-Aldrich). After filtration through a 70-µm cell strainer (BD Falcon, NJ, USA) to eliminate any tissue residue, the solution was centrifuged, and the supernatant layer was discarded. The cell pellets were then resuspended in DMEM (Gibco) containing 10% fetal bovine serum (FBS, Gibco) and seeded in 100 mm tissue culture dishes. The cells were cultured at 37 °C in a humidified 5% CO_2 incubator. After 48 h, the suspended cells were discarded, and the medium was replaced. The remaining cells were detached and passaged to 80% confluence using 0.25% trypsin–EDTA (Gibco). Figure 1 provides a schematic diagram of the study design.

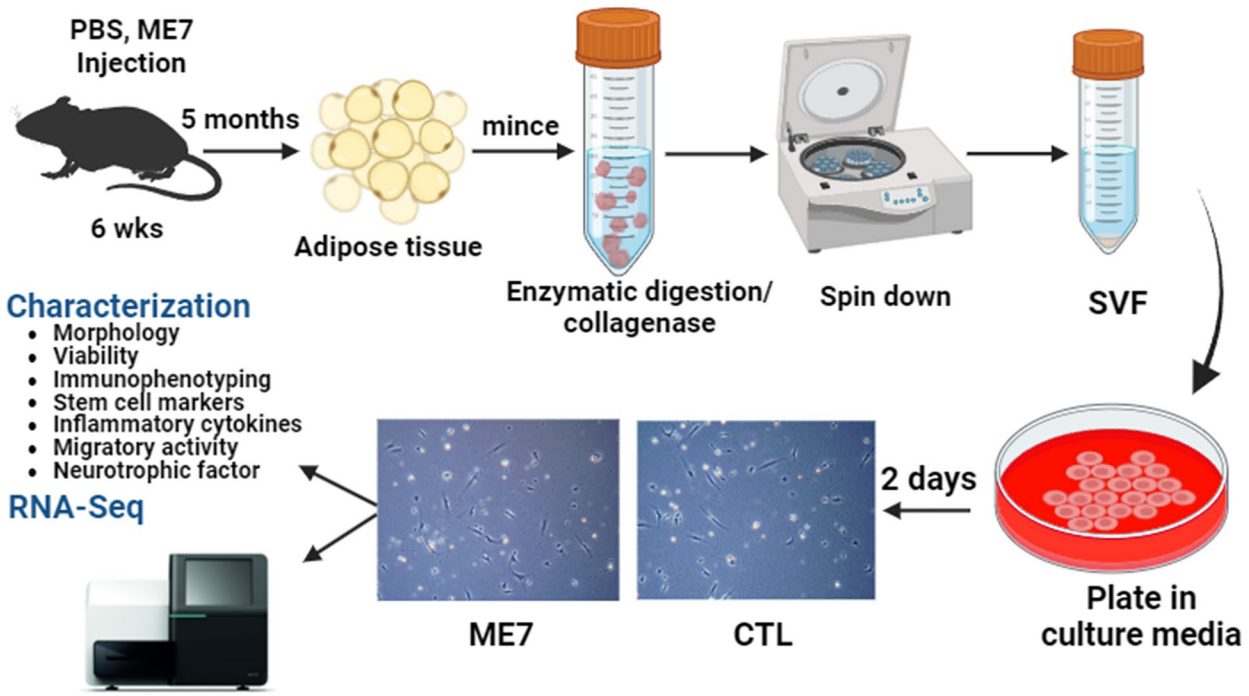

Fig. 1 Schematic diagram of the study design. PBS, phosphate-buffered saline; ME7, mouse-adapted scrapie prion strain; SVF, stromal vascular fraction. This figure was created using BioRender

Nuclear/cytoplasmic staining and CCK8 assay

To evaluate the morphology of AdMSCs isolated from ME7-infected and negative control mice, 5 µg of a wheat germ agglutinin–Alexa Fluor 488 conjugate (Life Technologies, Grand Island, NY, USA) was used to stain the cytoplasm for 10 min, as shown previously [12]. After being washed, the cells were mounted with Slow Fade Gold antifade reagent (Life Technologies), and images were obtained using a laser scanning confocal microscope (Carl Zeiss LSM 880, Oberkochen, Germany). The ImageJ software (version 1.52, imagej.nih.gov) was used to measure the average cell size from a total of 4 field images for 3 separate wells, resulting in a total of 60 randomly selected cells for each group.

To assess the effects of ME7 infection on AdMSC viability, AdMSCs (1×10^4 cells/well) were seeded in 96-well plates in basal growth medium for 24, 48, and 72 h. The viability of the AdMSCs was verified using a cell counting kit-8 (CCK8, Abcam, Cambridge, UK) according to the manufacturer's instructions. A microplate spectrometer (Molecular Devices, CA, USA) was used to measure the absorbance of viable cells at 450 nm.

Flow cytometry

A flow cytometric analysis was performed in AdMSCs using a cluster-of-differentiation (CD) antigen–antibody panel. Briefly, a cell suspension at passage 2 containing 5×10^5 cells was collected in 1× fluorescence-activated cell sorting (FACS) buffer (PBS with 0.1% bovine serum albumin) (Fisher Scientific). After blocking the Fc receptors with Fc block (BD Bioscience, Grand Island, NY, USA) for 20 min on ice, we treated the cells with 100 µl of FACS buffer containing one of the following antibodies for 1 h at 4 °C: FITC-conjugated anti-mouse CD105, CD90, CD44, or CD34 (BD Bioscience). The cells were subsequently washed and analyzed with flow cytometry (BD Biosciences). As a control, suitable isotype antibodies were used. Mean fluorescence intensity (MFI) and the percentage of marker-positive cells were analyzed using CellQuest software (Becton Dickinson, Mountain View, CA, USA).

Reverse transcriptase quantitative polymerase chain reaction (RT-PCR) analysis

RNA was extracted from AdMSCs using TRIzol reagent (Invitrogen, MA, USA) with the standard protocol [36]. Using 1 µg of total RNA, first-strand cDNA was generated by reverse transcription with ReverTra Ace-α (Toyobo, Tokyo, Japan) following the manufacturer's instructions. The reverse-transcribed products were amplified by the SYBR method using a CFX96 real-time PCR system (Bio-Rad, CA, USA) according to the manufacturer's instructions. The incorporation of SYBR green dye (Yuseong-gu, Daejeon, Republic Korea) into the PCR products was monitored in real time with a CFX96 PCR system. The relative mRNA expression of stem cells and neuroinflammation and neurotrophic factors were examined after normalization to the expression of reference gene *ACTN*. The complete list of primers for all genes and *ACTN* is presented in Supplementary Table 1.

Immunofluorescence of cells

The CXCR4 expression profiles in the two types of AdMSCs were assessed by immunofluorescence staining. AdMSCs were cultured in chamber slides (SPL Life Sciences Co., Gyeonggi-do, Korea) at a density of 2×10^4 cells/ml. The cells were fixed in 4% paraformaldehyde, and washed with PBS, before being permeabilized for 10 min at RT using 0.1% Triton X-100. The cells were then blocked with Power Block (BioGenex Laboratories, CA, USA) for 30 min at RT and incubated overnight with a CXCR4 antibody (1:100, ab124824, Abcam). The cells were then treated with an anti-rabbit Alexa Fluor-647 (Cell Signaling Tech., MA, USA) for 1 h at RT. Cells were mounted using ProLong Gold Antifade Mounting media with DAPI (Invitrogen, MA, USA). Images were collected and processed using a fluorescence microscope (Zeiss Axio-Imager M2, Oberkochen, Germany), and all images were taken under the same conditions. The fluorescence intensity was measured using ImageJ software (NIH, Bethesda, MD, USA).

Transwell migration assay

The two sets of AdMSCs were assessed for migration activity using a Transwell membrane system (Corning, NY, USA) in 24-well plates as previously described [37]. Ten percent FBS was used in the lower chambers and 1×10^5 AdMSCs were placed in each upper chamber resuspended in 100 µl serum-free DMEM. DMEM only was used as a negative control in the lower chamber. After 24 h, the cells that migrated to the membrane's lower surface were fixed using 4% paraformaldehyde and subsequently stained with 0.2% crystal violet stain. Following washing, cells in four random fields (×100 magnification) were counted for statistical analysis.

Scratch wound assay

In vitro wound healing was assessed using a cell scratch assay, following previously established protocol [38]. Confluents in the two sets of AdMSCs at passage 2 were subjected to a scratch using a sterile 200 µl pipette tip. The monolayers were subsequently washed twice with PBS to eliminate debris. Wound photographs were captured immediately following the initial lesion (time zero) and after a 24-h healing period. Measurements were conducted using ImageJ software, and the percentage of

wound closure was calculated by determining the difference between the scratched area at time zero and that obtained after 24 h.

Library construction and RNA-Seq

Three replications for each sample (negative control and ME7-infected) were used for RNA extraction by TRIzol reagent. The RNA samples were treated with DNase I (New England Biolabs, Ipswich, MA, USA) to remove genomic DNA. The concentration and quality of the extracted RNA were determined using a Quant-iT RiboGreen RNA assay kit (Invitrogen, cat.# R11490) and a 4200 TapeStation system (Agilent Technologies, Part# G2991BA, Santa Clara, CA, USA), respectively. Samples with RNA integrity number values higher than 9 were used to create the libraries using an Illumina TruSeq RNA library kit (Illumina Inc., San Diego, CA, USA) with Ribo-Zero H/M/R_Gold according to the manufacturer's instructions. The quality and yield of the prepared libraries were assessed using a D1000 TapeStation system (Agilent Technologies). Using an Illumina HiSeq 2000, the libraries were sequenced with 100 bp paired-end reads per sample (Macrogen, Seoul, Korea).

Sequence annotation and identification of differentially expressed genes (DEGs)

Quality control checks of the raw data sequencing were conducted with FastQC (v0.11.7, Babraham Institute, http://www.bioinformatics.babraham.ac.uk/projects/fastqc/) to evaluate sequence yield, base quality, GC profile, k-mer distribution, overrepresented sequences, and primer contamination. The trimmomatic program (v0.38, http://www.usadellab.org/cms/?page=trimmomatic) was used to remove adapter sequences and low-quality bases. The remaining reads were mapped to the HISAT2 mouse reference genome (v2.1.0, https://ccb.jhu.edu/software/hisat2/index.shtml), and the known genes and transcripts were assembled with StringTie (https://ccb.jhu.edu/software/stringtie/) based on the reference genome model. After assembly, the abundance of genes and transcripts in each sample was calculated in the read count and normalized as fragments per kilobase of transcript per million mapped reads and transcripts per kilobase million, respectively. To display the DEG expression patterns, a hierarchical clustering analysis was performed using complete linkage and Euclidean distance as a measure of similarity.

Gene ontology (GO) and enrichment analyses

To identify functional groups and pathways, GO (http://geneontology.org/) and Kyoto Encyclopedia of Genes and Genomes (KEGG, http://www.genome.jp/kegg/) pathway analyses were performed. The GO terms were classified into three subgroups: biological process, cellular component, and molecular function. For functional enrichment analysis, all DEGs were mapped to terms in the GO databases, and significantly enriched GO terms were searched among the DEGs using $p < 0.05$ as the threshold.

Validation of gene expression by RT-PCR

To validate the reliability of the DEG results, the expression levels of the selected transcripts were determined by RT-PCR. Total RNA from AdMSCs at passage 3 was extracted using TRIzol, and cDNA was synthesized as described above. The amplicons were generated using primers listed in Supplementary Table 1.

Statistical analysis

For statistical analyses, SPSS 25.0 (IBM, Armonk, NY) was used. Students' t-test and one-way analysis of variance with post-hoc Tukey testing were performed. The following p-values indicate statistical significance in all figures: * $p < 0.05$, ** $p < 0.01$, and *** $p < 0.001$. The results are displayed as mean ± standard deviation (SD) of experiments carried out in triplicate.

Results

Detection of PrP^{Sc} and GFAP

Our previous study showed that a prion disease model using ME7 scrapie strain demonstrates common characteristics of prion disease, including weight loss, abnormal behaviors, and mortality in mice [39]. In the current study, to establish a prion-infected mouse model, we injected mice with the terminally ill ME7 scrapie strain. Five months post-injection, brain homogenates from negative control and ME7-infected mice showed similar levels of total PrP (Fig. 2A). The abnormal folding of PrP^{C} into amyloid fibrils, known as PrP^{Sc}, is directly related to prion diseases [4]. As a result, Western blotting, the most commonly used method for detecting PrP^{Sc} [40], was used. Here, PrP^{Sc} in the brain homogenates of ME7-infected mice was readily detected by standard immunoblotting, while homogenates of brain tissue from the wild-type mice did not exhibit PrP^{Sc} bands (Fig. 2A). Various studies have demonstrated elevated GFAP levels, a marker of astrocyte activation, in prion disease [41]. Consequently, we assessed GFAP levels using immunoblot analysis. The findings indicated that GFAP levels in brain homogenates from ME7-infected mice were significantly higher than those from the negative control mice (Fig. 2B, C, $p < 0.001$). In summary, we successfully created a prion disease model utilizing the terminal stage of the ME7 scrapie strain.

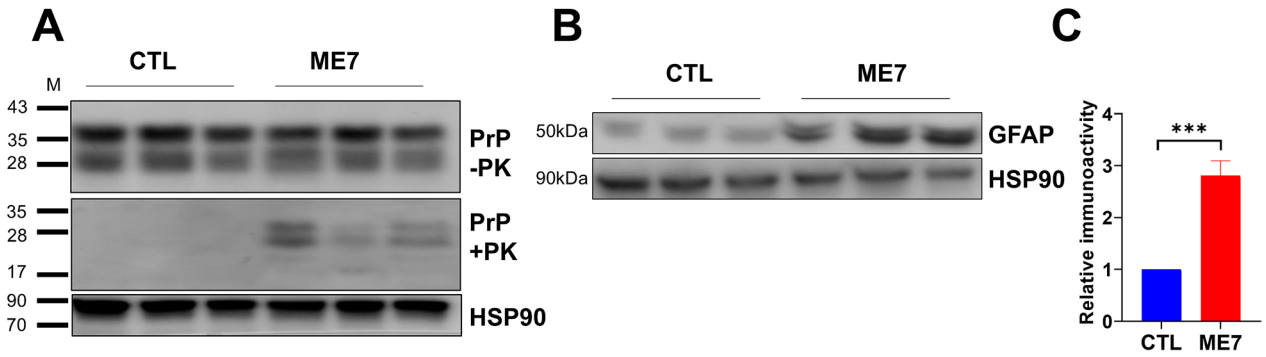

Fig. 2 Characteristics of the ME7 prion disease model. **A** Representative western blot analysis of total prion protein (PrP) and the abnormal isoform of PrP (PrP^{Sc}) in brain homogenates from ME7-infected and negative control mice (CTL, n = 3 per group) at 5 months post-injection. PrP-PK, no proteinase K treatment; PrP + PK, proteinase K treatment. **B** GFAP immunoblots analyzed by Western blotting (n = 3 per group). **C** Quantitative analyses of GFAP immunoblots from the experiments panel. ***$p < 0.001$. HSP90 served as the loading control. All data are expressed as the means ± SD. The student's t-test was used to compare two groups. The full-length blot is presented in supplementary Figs. 1 and 2

Effects of ME7 infection on the morphology and viability of AdMSCs

The morphological characteristics and viability of MSCs are crucial, as they influence the cells' ability to regenerate tissues and differentiate into specific cell lineages [11]. Therefore, the morphology of AdMSCs from ME7-infected and negative control mice was investigated, revealing a pronounced adhesion growth (Fig. 3A). The effect of ME7 infection on cell morphology was significantly increased cell size (Fig. 3A,B $p < 0.05$) compared with AdMSCs isolated from the negative control, which had a spindle-shape and a fibroblast morphology (Fig. 3A). To examine the effect of ME7 infection on AdMSC viability, we used a CCK8 kit. AdMSCs isolated from ME7-infected mice showed decreased proliferative capacity at 24, 48, and 72 h compared with AdMSCs isolated from the negative control ($p < 0.05$, $p < 0.01$, and $p < 0.05$, respectively) (Fig. 3C).

Immunophenotyping

According to the minimal criteria for defining MSCs [42], AdMSCs isolated from ME7-infected mice and negative controls were characterized by flow cytometry analysis. The identification of MSCs was based on the presence of specific mouse MSC surface markers and the absence of surface markers associated with the hematopoietic cell lineage. Flow cytometric analyses of AdMSCs isolated from negative control and ME7-infected mice revealed > 80% expression of the MSC markers CD90 and CD44. Both cell types showed mild expression of CD105, and both sets of MSCs exhibited very low expression of CD34, which is generally associated with hematopoietic cells (Fig. 3D). In fact, mouse AdMSCs partially express CD105, unlike human MSCs [43]. The average percentage or MFI of each marker did not differ significantly between negative control and ME7-infected samples (Fig. 3E, F), suggesting a typical MSC phenotype.

Expression of stem cell markers, inflammatory cytokines, and neurotrophic genes

To gain further insight into the effects of ME7 infection on the characterization of AdMSCs, we investigated the expression of stem cell markers, inflammatory cytokines associated with prion disease, and neurotrophic genes. When the mRNA expression of stem cell markers was compared between AdMSCs isolated from negative control and ME7-infected mice, *CXCR4*, a stem cell marker, was significantly downregulated in those from ME7-infected mice ($p < 0.05$); the remaining markers did not differ between the conditions (Fig. 4A). CXCR4 signaling has been shown to play a key role in the migratory functions of AdMSCs [44]. We confirmed the decreased expression of CXCR4 through immunofluorescence staining, which revealed that the immunofluorescence signal for CXCR4 in the control-AdMSCs was significantly greater than in the ME7-infected-AdMSCs (Fig. 4B, C $p < 0.001$). To study how ME7 infection impacts the migration abilities of AdMSCs, Transwell migration and scratch wound assays were conducted. The findings from the Transwell migration assay indicated that the migratory capacity of AdMSCs obtained from negative controls was significantly greater than that of AdMSCs derived from ME7-infected mice (Fig. 4D, E $p < 0.001$). There was no significant difference in the migration of AdMSCs toward FBS free medium alone (Fig. 4D, E). The findings from the scratch wound assay were consistent with those observed in the Transwell migration assay (Fig. 4F, G $p < 0.05$).

The mRNA expression of genes linked to prion disease was assessed in AdMSCs isolated from both the

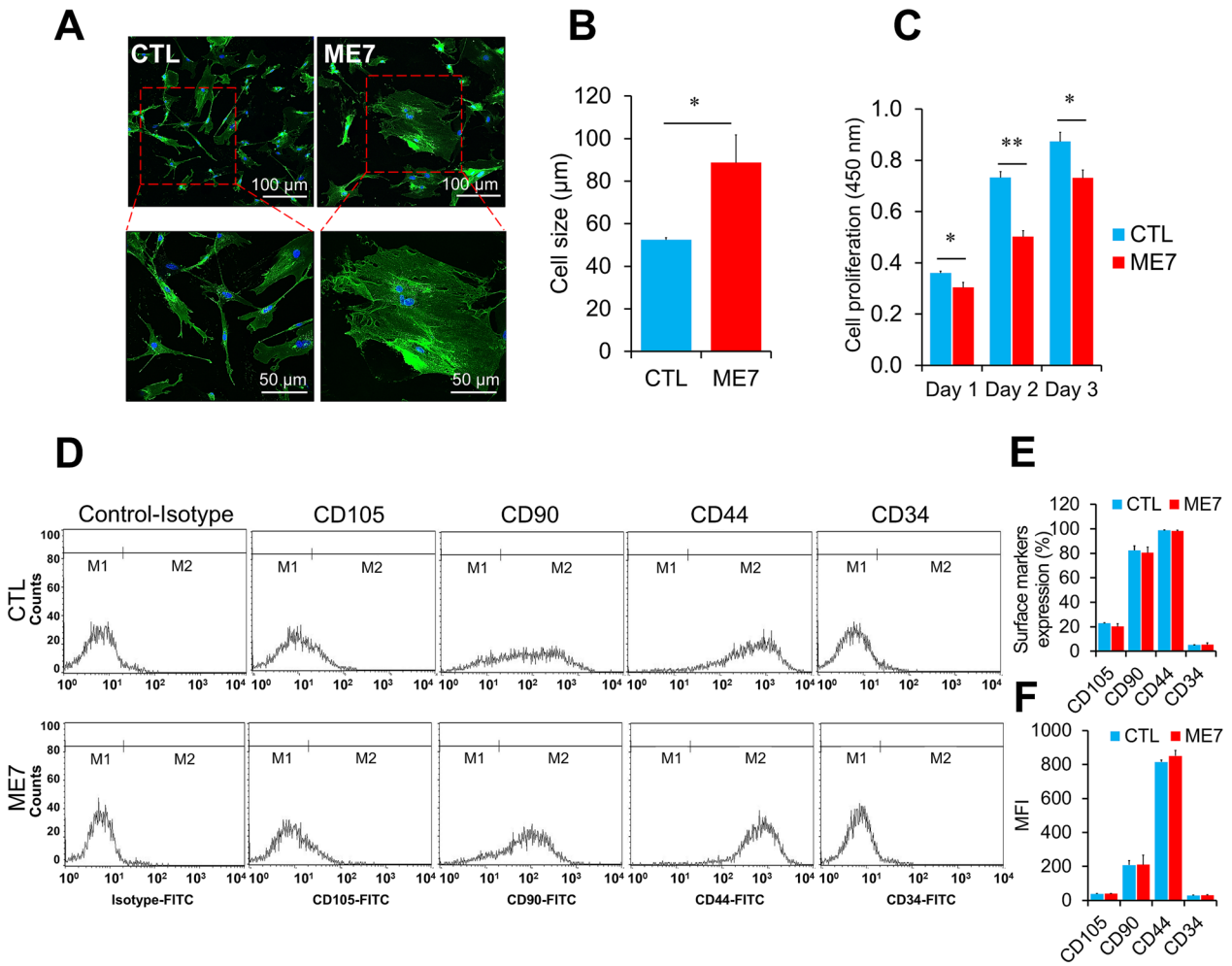

Fig. 3 Properties of adipose-derived mesenchymal stem cells (AdMSCs) isolated from ME7-infected mice compared with the negative control. **A** Representative images of morphology (from one of four independent experiments) show changes in cell size due to ME7 infection (upper panel, low magnification and lower panel, high magnification). **B** Measurement of cell size shows a significant increase in the diameter of AdMSCs isolated from ME7-infected mice compared with the negative control group (n = 5). * $p < 0.05$. All data are expressed as the means ± SD. The student's t-test was used to compare two groups. **C** Viability of AdMSCs from ME7-infected and negative control mice. * $p < 0.05$, ** $p < 0.01$. All data are expressed as the means ± SD. The student's t-test was used to compare two groups. **D** Characterization of AdMSCs with flow cytometry through an immunophenotype analysis of MSC cell surface markers (CD105, CD90, and CD44) and a hematopoietic marker (CD34) (n = 3). **E** Percentage means of MSC markers from the two groups (n = 3). **F** Mean fluorescence intensity (MFI) of MSC markers from the two groups (n = 3). All data are expressed as the means ± SD. The student's t-test was used to compare two groups

negative control group and ME7-infected mice. The analyzed genes included *CCL5, TNF-α,* complement protein *C3,* and *IL6,* which are known contributors to the development of neurotoxic reactive astrocytes [45]. Compared with the negative control, the mRNA expression of inflammatory markers of astrogliosis (*CCL5, TNF-α, C3,* and *IL6*) was upregulated in ME7-infected AdMSCs ($p < 0.05$) (Fig. 4H). The expression of the neurotrophic factor *BDNF* was lower in ME7-infected AdMSCs than in the negative control, but the difference was not significant ($p = 0.08$) (Fig. 4I).

RNA-Seq analysis

To investigate how ME7 infection translates into variations in the gene expression of AdMSCs, the complete transcriptome of AdMSCs was profiled (Fig. 5A). To visualize transcriptomic differences between ME7-infected AdMSCs and the negative control, a heatmap was generated showing values of |log2 (fold-change)| > 1 (log2FC) (Fig. 5B). Those results show the modulation effect of ME7 infection: gene regulation was significantly altered, with 367 genes differentially expressed (190 upregulated and 177 downregulated) between AdMSCs isolated from

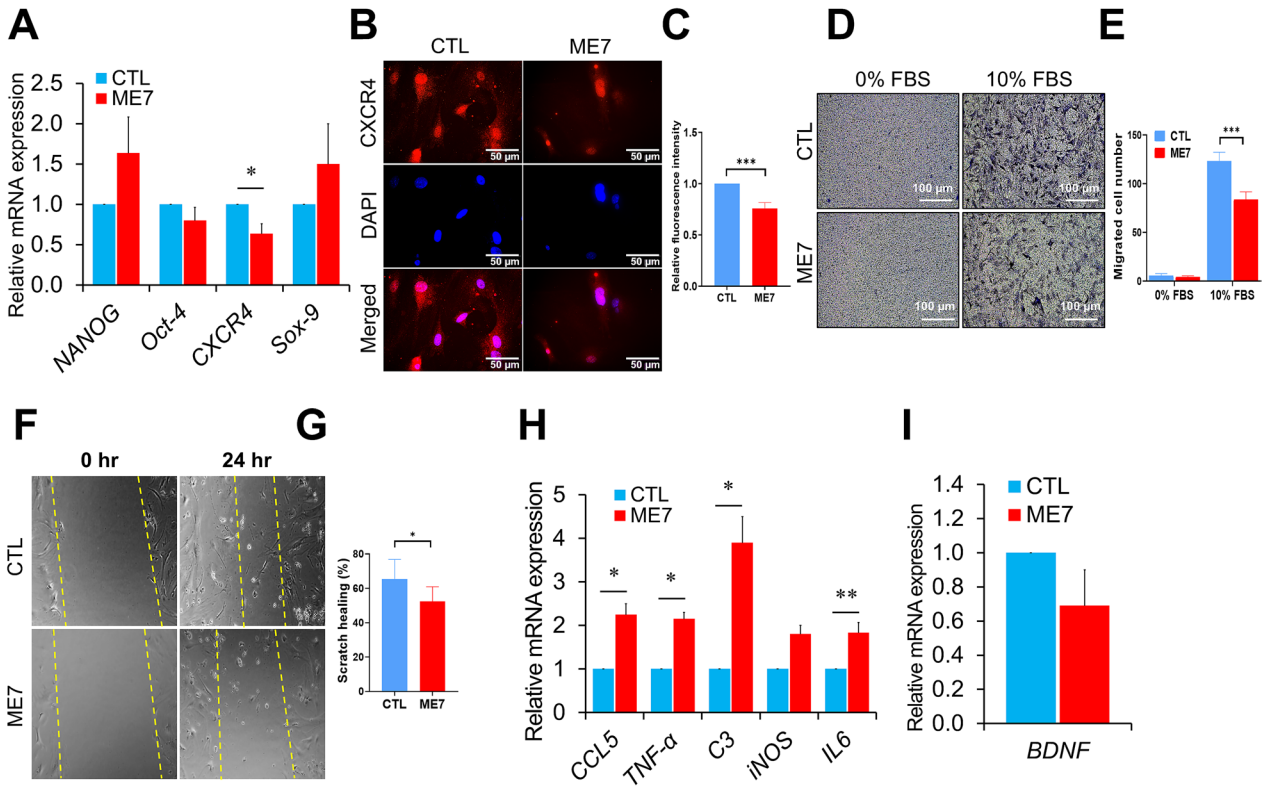

Fig. 4 Gene expression of stem cell markers, inflammatory cytokines, neurotrophic factors and the migration activity (**A**) Gene expression of *NANOG, Oct-4, CXCR4,* and *SOX-9.* **p* < 0.05. All data are expressed as the mean ± SD (n = 3). The student's t-test was used to compare two groups. **B** Representative immunofluorescent images of CXCR4 staining on AdMSCs from ME7-infected and negative control (CTL) mice. CXCR4 was detected using an anti-CXCR4 antibody (red), and nuclei was counterstained with DAPI (blue). Scale bars are 50 µm. **C** Quantitative analysis of CXCR4 fluorescence intensity. ****p* < 0.001. All data are expressed as the means ± SD (n = 3). The student's t-test was used to compare two groups. **D** Transwell migration assay showed a decrease in the number of migrated AdMSCs in ME7-infected group compared to the control group. **E** Statistical analysis of migration activity after 24 h. ****p* < 0.001. All data are expressed as the means ± SD (n = 3). The student's t-test was used to compare two groups. **F** Scratch assay of AdMSCs for 24 h. Photographs were taken at 0 and 24 h after scratching. Scale bars are 100 µm. **G** Statistical analysis of wound healing. **p* < 0.05. All data are expressed as the mean ± SD (n = 3). The student's t-test was used to compare two groups. **H** Gene expression of *CCL5, TNF-α, C3, iNOS,* and *IL6.* **I** Gene expression of *BDNF*. **p* < 0.05 and ***p* < 0.01. All data are expressed as the mean ± SD (n = 3). The student's t-test was used to compare two groups

ME7-infected mice and those from the negative controls (Supplementary file 1). A volcano plot was created based on the threshold value of the fold change. In the volcano plot in Fig. 5C, all DEGs are shown in orange (upregulated) or blue (downregulated). The number of genes has also been presented (Fig. 5D).

DEG identification and functional enrichment

We next categorized highly DEGs from ME7 and negative control AdMSCs according to the following GO classification terms: biological process, cellular component, and molecular function. The top 10 GO term enrichments for each GO category (biological process, cellular components, and molecular function) are presented in order of significance ($p < 0.001$) in Fig. 6A. The categories with the highest gene counts in the biological process field were negative regulation of locomotion, extracellular matrix (ECM) organization, and extracellular structural organization, as shown in Fig. 6Aa. The top three categories in the cellular component section were genes involved in the basal part of the cell, the apical plasma membrane, and collagen-containing ECM (Fig. 6Ab). The most widely dispersed genes in terms of molecular function were related to amide binding, peptide binding, and structural components of the ECM (Fig. 6Ac).

To evaluate the enrichment in signaling pathways, we performed a KEGG pathway analysis, which includes metabolism, genetic information processing, environmental information processing, cellular processes, organismal systems, and human disease (Fig. 6B, C). In the comparison between AdMSCs isolated from ME7-infected mice and those from the negative controls, pathways categorized in the PI3K-Akt signaling pathway, cell adhesion molecules, protein digestion and absorption,

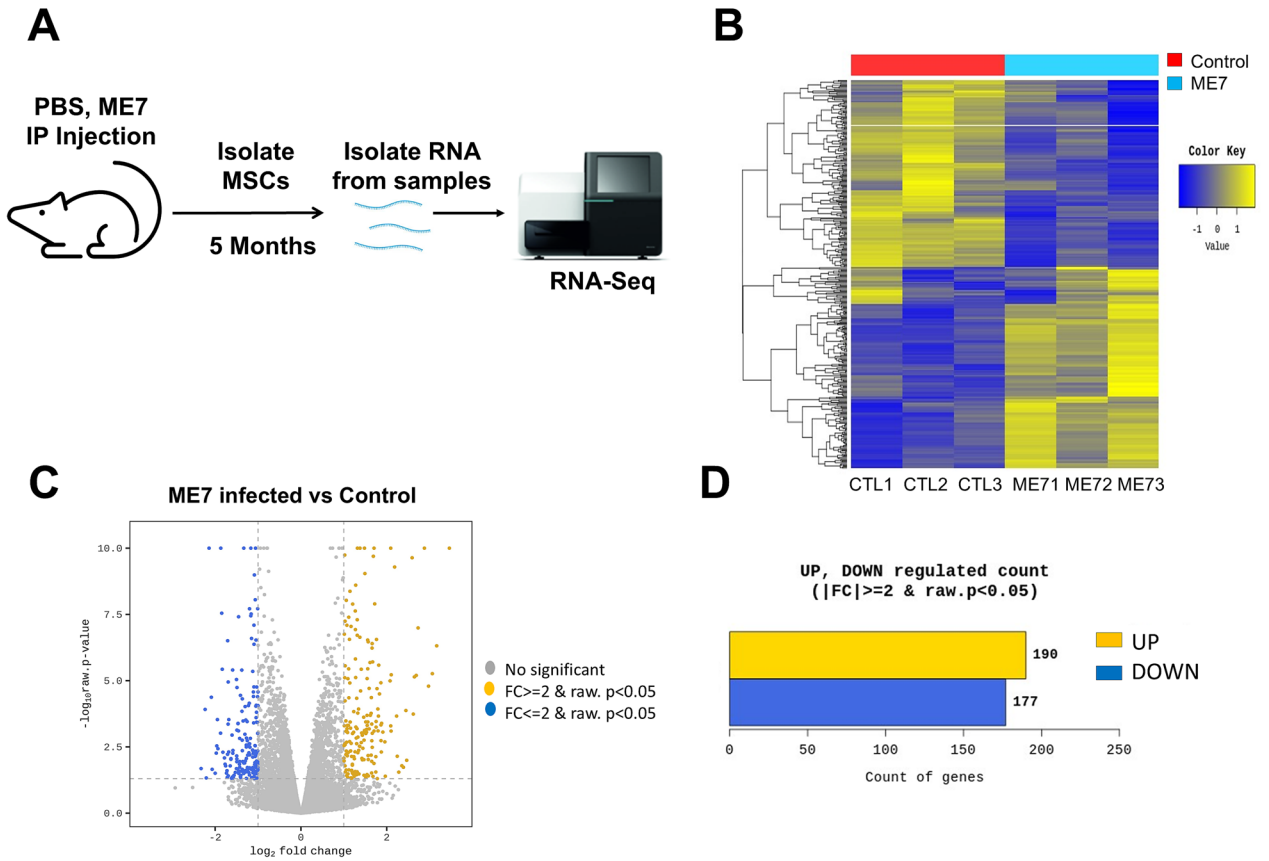

Fig. 5 **A** Diagram of the prion mouse model and RNA-Seq experiment. **B** Heatmap of differentially expressed genes (DEGs) between adipose-derived mesenchymal stem cells (AdMSCs) isolated from ME7-infected mice and those from negative controls. Yellow stripes in the figure represent high-expression genes, and blue stripes represent low-expression genes. **C** Volcano plot of DEGs and the number of up- and downregulated genes based on fold changes and *p-values*. Significantly upregulated genes (adjusted *p-value* ≤ .05 and log2(FC) > 1) are in orange; significantly downregulated genes (adjusted *p-value* ≤ .05 and log2(FC) < 1) are in blue (**D**)

cytokine–cytokine receptor interaction, and human papillomavirus infection showed high enrichment among the log2FC upregulated genes (Supplementary file 2) (Fig. 6B, C). Collectively, these findings provide further evidence that ME7 infection may negatively impact AdMSCs.

Validation of RNA-Seq by RT-PCR

The inflammatory response associated with prion disease is increased, as indicated by elevated levels of various cytokines. Among these cytokines, which contribute to the development of prion diseases through direct or indirect interactions, are *Ccl11, Cyp7b1, Dio3, Hp,* and *TNFSF8* [46–49]. To validate the RNA-Seq findings of these genes with significance at log2FC ≤ −2 or ≥ 2, RT-PCR was used. Those analyses confirmed the overexpression of *Ccl11, Cyp7b1, Dio3, Hp,* and *TNFSF8*, originally detected in the RNA-Seq, in AdMSCs from ME7-infected mice compared with the negative control AdMSCs (Fig. 7A). The haptoglobin (*Hp*) gene was the top DEG (11-fold increase) in ME7-infected AdMSCs vs. the negative controls. *Hp* plays an important role in cellular iron storage via hemoglobin-dependent pathways [50]. Therefore, we further investigated *hepcidin*, the central regulator of systemic iron homeostasis [51]. As shown in Fig. 7B, AdMSCs from ME7-infected mice demonstrated upregulation of the *hepcidin* gene relative to controls, suggesting the underlying mechanism of iron accumulation and associated toxicity in prion disease [52, 53].

Discussion

Disruption of biological networks causes activation of several pathogenic processes during disease development. Prion disorders cause alterations in the expression of hundreds of genes and cellular processes, such as PrP^{Sc} accumulation, microglial/astrocytic activation, synaptic degeneration, and neuronal cell death [54]. MSCs are a promising candidate for cell-based therapy to treat neurodegenerative diseases, including prion diseases [15, 55, 56]. However, individuals who stand to benefit from stem

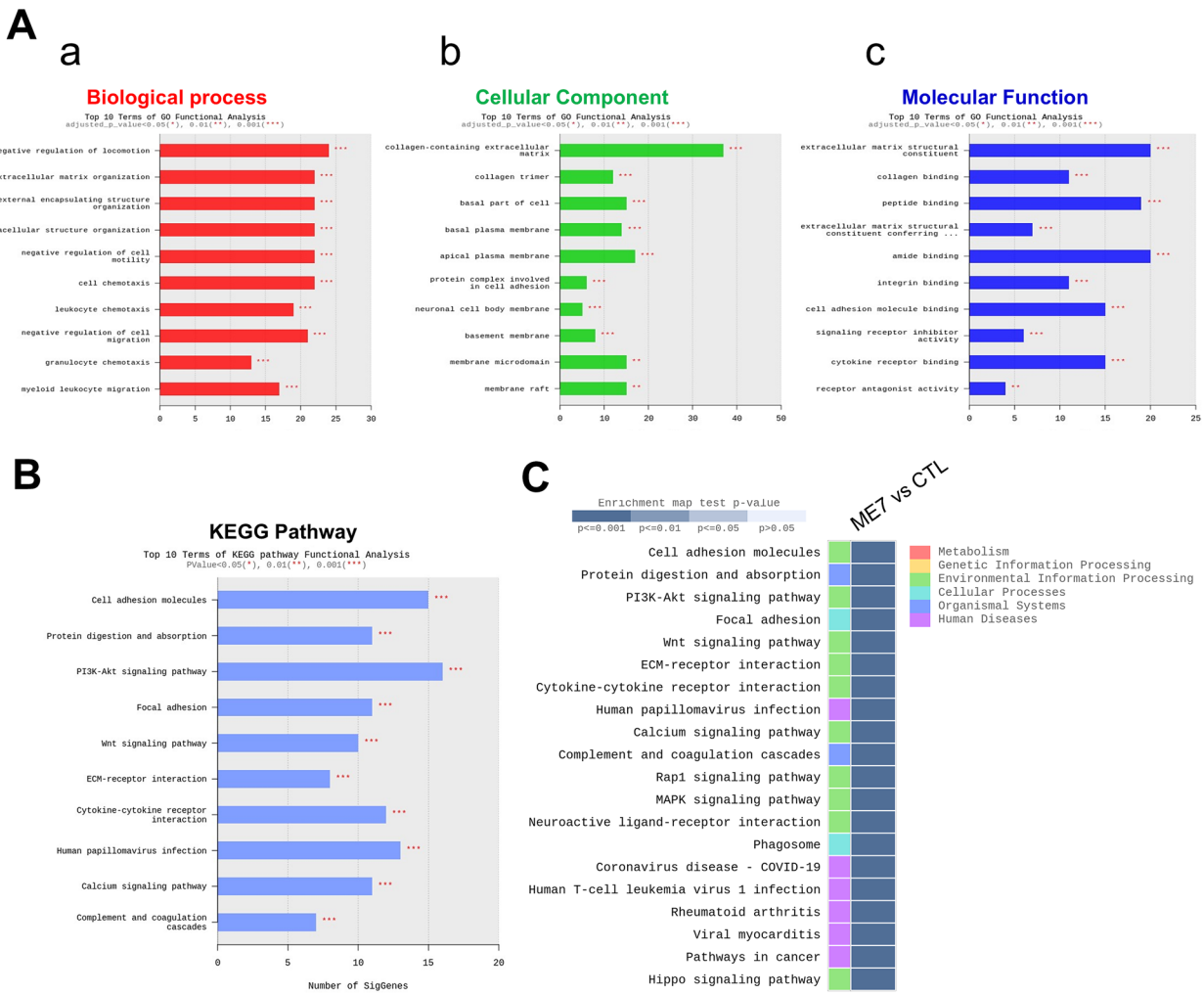

Fig. 6 Functional classification of gene ontology (GO) enrichment clusters. **A** The 10 most significant pathways of differentially expressed genes (DEGs) terms between adipose-derived mesenchymal stem cells (AdMSCs) isolated from ME7-infected mice and those from negative controls were annotated according to ontology category: a. biological process, b. cellular component, and c. molecular function. X- and Y-axes indicate the number of DEGs and GO-term gene classification, respectively (***$p < 0.001$). **B** Significant KEGG functional pathways and (C) a heatmap of the enriched KEGG pathways (***$p < 0.001$)

cell treatments often present with coexisting systemic disorders that could impair the ability of their own stem cells to function in autologous transplantation [57]. It is recommended that the cellular characteristics, including an entire transcriptome analysis, of MSCs from a model of prion infection be completed before clinical application to optimize clinical outcomes. We hypothesized that prion infection might alter the transcriptome of AdMSCs. To identify the related underlying processes, we concentrated on a transcriptome analysis using the RNA-Seq technique.

Initially, we assessed the characteristics and phenotypic distinctions of AdMSCs isolated from ME7-infected and negative control mice. We found that AdMSCs isolated from ME7-infected mice had lower viability and larger cell sizes, hallmarks of cellular senescence [58]. Similar observations of reduced growth potential have been reported in MSCs derived from patients with other neurodegenerative diseases, such as multiple sclerosis [59] and amyotrophic lateral sclerosis [60]. Furthermore, it has been reported that BM-MSCs isolated from animals with scrapie prion infection showed a significant decrease in viability compared with the controls [24]. That diminished growth potential has been suggested to indicate that prion infection modulates MSCs in ways that lead to apoptotic cell death and senescence through autonomous and non-autonomous mechanisms [39]. These characteristic results are consistent with RNA-Seq

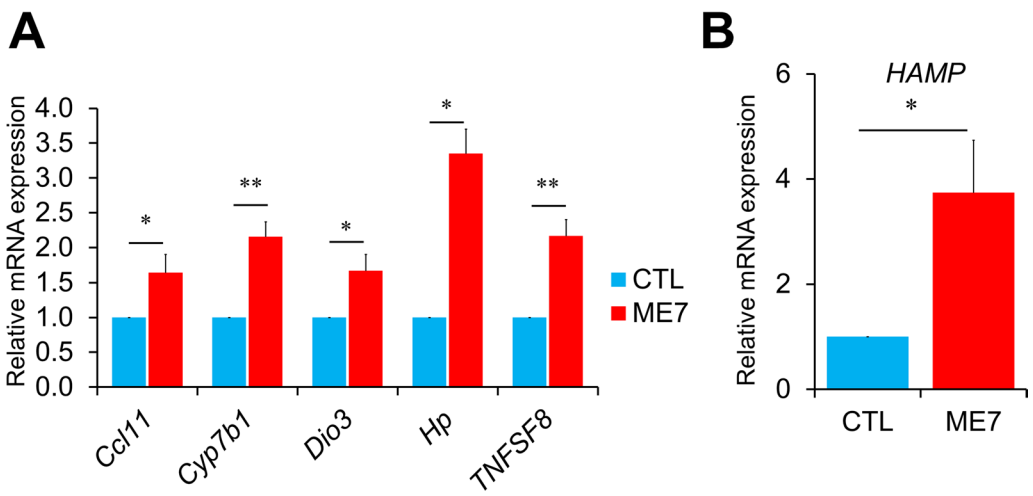

Fig. 7 Validation of RNA-Seq analysis (**A**) The relative expression levels of *Ccl11*, *Cyp7b1*, *Dio3*, *Hp,* and *TNFSF8* were analyzed in adipose-derived mesenchymal stem cells (AdMSCs) isolated from ME7-infected and negative control mice. Reverse transcription-polymerase chain reaction was performed to confirm the increase in the expression of those genes in AdMSCs. **B** The relative expression levels of *HAMP* was analyzed in AdMSCs isolated from the two groups. All data are expressed as the means ± SD (n = 3). The student's t-test was used to compare two groups; * $p < 0.05$ and ** $p < 0.01$ compared with the corresponding control. *Ccl11*, C–C motif chemokine 11; *Cyp7b1*, cytochrome P450 family 7 subfamily B member 1; *Dio3,* iodothyronine deiodinase 3; *Hp*, Haptoglobin; *TNFSF8,* tumor necrosis factor superfamily member 8. *HAMP*, hepcidin antimicrobial peptide

data that showed upregulation of growth arrest–specific genes, *Gas1* and *CCN5,* and a gene associated with apoptosis, caspase-12, in AdMSCs isolated from ME7-infected mice, implicating the dependent pathway in neurodegenerative prion disease [61]. AdMSCs from both negative control and ME7-infected mice expressed the MSC surface markers CD105, CD90, and CD44 in flow cytometry, confirming their "stemness" [12].

Transplanted MSCs have demonstrated their ability to migrate to brain regions affected by prions, driven by the release of trophic factors that promote endogenous healing processes in the damaged brain [62]. CXCR4 signaling plays an important role in the regulation of stem cell migration and development [63, 64]. Our research revealed that AdMSCs isolated from ME7-infected mice exhibited a significantly reduced CXCR4 expression compared to negative control group. We further evaluated the migratory capabilities of both groups of AdMSCs through Transwell migration and scratch wound assays, which showed that ME7 infection negatively affected the migration of AdMSCs. Overall, this reduced CXCR4 expression may impair the therapeutic potential of AdMSCs in autologous transplantation scenarios.

Additionally, we measured the mRNA expression of genes correlated with prion disease in AdMSCs and found significant increases in inflammatory cytokines such as *CCL5*, complement protein *C3, TNFα,* and *IL6*. Those upregulated genes are associated with reactive astrocytes [45, 65]. Modulations of *BDNF* and its signaling pathway in prion disease have been studied previously and demonstrated downregulation [66]. In our results, gene expression of *BDNF* decreased in AdMSCs isolated from ME7-infected mice, but the difference was not significant. This result is evidence that prion infection has adverse effects on AdMSCs and affects the potential use of autologous AdMSCs for therapy.

Prion disease is a gene-related disease [67]. Growing evidence suggests that various genes and cellular pathways are involved in the onset and progression of CJD [68]. However, AdMSC transcriptional alterations in response to prion infection have not been fully characterized. In our study, we used RNA-Seq to identify DEGs in AdMSCs isolated from prion-infected mice. We found that many genes were differentially expressed between AdMSCs from ME7-infected mice and those from negative controls. Our GO analyses highlighted the upregulation of biological processes such as ECM organization, extracellular structural organization, ECM structural constituents, and external encapsulating structure organization. ECM changes were previously described in prion diseases to increase PrP^{Sc} deposition [69]. Collagen has been shown to have significant association with prion accumulation [70]. Various types of collagen, including *COL1A1* and *COL3A1,* have been found to be induced in multiple sclerosis lesions [71] and implicated in promoting Alzheimer's-like disease in mice [72]. Our results indicate the upregulated expression of several collagen genes (*COL14A1, COL6A2, COL28A1, COL3A1,*

COL15A1, COL24A1, and *COL8A2*) in AdMSCs isolated from ME7-infected mice, suggesting their involvement in molecular function and cellular components. In addition, a subset of genes associated with the innate immune response and inflammation, such as chemokines and cytokines, has been implicated in prion diseases [73–75]. This association might be the result of an inflammatory response to brain injury, which often manifests as microglial activation and astrogliosis [76]. Therefore, specific treatments to reduce inflammation are promising approaches for prion disease [77, 78]. Functional analysis of our RNA-Seq data revealed an enhanced inflammatory response in AdMSCs isolated from ME7-infected mice through an increase in chemotaxis production and cytokine-mediated receptors. In particular, *PTGDR2* is involved in a wide variety of neurophysiological functions [79]. The upregulation of *INAFM1, TNFSF8, TGTP1, IFNLR1, Ccl3, Ccl8, IL1RN, MMP3,* and *Ccl11* was detected in the present DEG results, and previous studies have shown potential associations between those genes and prion diseases or other neurodegenerative disorders [49, 80, 81]. Our data indicate a high likelihood of PrP^{Sc} deposition in MSCs from prion-infected donors, as reported previously in vitro [25]. Also, these results might explain the incomplete therapy and PrP^{Sc} accumulation observed from the autologous use of MSCs for prion disease [82]. We selected DEGs (*Ccl11, Cyp7b1, Dio3, Hp,* and *TNFSF8*) for further analysis by RT-PCR and observed consistent fold changes in their expression between the RNA-seq and RT-PCR analyses, confirming the validity of both the RNA-seq data and the alignment analysis.

PrP^{C} was modeled to have a role in iron homeostasis because PrP^{C} knockout mice exhibited reduced iron uptake and transport [53]. An imbalance in brain iron homeostasis is significantly associated with neurotoxicity in prion-infected cell and mouse models [52, 83]. Here, significant GO functional terms related to iron metabolism genes (*SLC38A4, SLC1A3, SLC16A12, Hp, NOXO1, SERPINA3N, SOD3, PTGDR2, Ccn5, DIO3, CYP7B1, Ccn3, CPXM2, CP, ITGA11, CSF2,* and *SPON2*) [84–86] were detected in AdMSCs isolated from ME7-infected mice. Interestingly, the *Hp* gene was the top DEG (11-fold increase) in ME7-infected mice compared with the negative controls. That encouraged us to look at the expression of *hepcidin*, encoded by the *HAMP* gene, as a central regulator of systemic iron homeostasis [86]. Those results demonstrated upregulation of *hepcidin* relative to negative controls. Chaudhary et al. showed that brain *hepcidin* contributes to neuronal iron accumulation and ROS-mediated toxicity in prion disease [83]. Ferroptosis, an iron-dependent form of regulated cell death, has recently been associated with neurodegenerative diseases [87]. The specific regulatory mechanisms of ferroptosis in prion diseases need to be explored. A limitation of the current study is that we used only the ME7 prion strain; thus, it is necessary to validate our study results with other prion strains.

Conclusions

In this study, we investigated the characterization and transcriptome profile of AdMSCs isolated from ME7-infected mice. These cells revealed a lower proliferation rate, upregulated inflammatory genes associated with reactive astrocytes, and downregulated expression of the stem cell marker *CXCR4* compared with basal levels. Furthermore, ME7 infection has a negative impact on the migratory activity of AdMSCs. The RNA-Seq analysis returned 367 DEGs between AdMSCs from ME7-infected mice and those from the negative controls. We also showed that iron metabolism modulators are involved in prion infection, suggesting that they play an important role in prion pathogenesis and neurotoxicity. Based on the current study results, autologous AdMSCs might not be suitable for MSC-based therapy for prion diseases.

Abbreviations

MSCs	Mesenchymal stem cells
AdMSCs	Adipose-derived mesenchymal stem cells
CJD	Creutzfeldt-Jakob disease
DEGs	Differentially expressed genes
GO	Gene ontology
KEGG	Kyoto encyclopedia of genes and genomes
CCK8	Cell counting kit-8
PrP	Prion protein
PrP^{Sc}	Pathological form of prion protein
PK	Proteinase K
ECM	Extracellular matrix
Hp	Haptoglobin
FACS	Fluorescence-activated cell sorting
RNA-Seq	RNA-sequencing
RT-PCR	Reverse transcription polymerase chain reaction
MFI	Mean fluorescence intensity

Supplementary Information

The online version contains supplementary material available at https://doi.org/10.1186/s13287-025-04273-x.

Supplementary file1 (XLSX 92 kb)
Supplementary file2 (XLSX 22 kb)
Supplementary file3 (TIF 2285 kb)
Supplementary file4 (TIF 2275 kb)
Supplementary file5 (DOCX 18 kb)

Author contributions

MZ, Y-CK, and B-HJ conceived and designed the study. MZ and Y-CK performed the experiments. MZ performed the data analyses and manuscript preparation. MZ and B-HJ wrote the manuscript. Y-CK and B-HJ revised the manuscript. All authors read and approved of the final manuscript.

Funding
This work was supported by National Research Foundation of Korea (NRF) grants funded by the Korean government (MSIT) (RS-2025–00517133, 2021R1 A2C1013213, 2022R1C1C2004792). This research was supported by the Basic Science Research Program through the NRF of Korea funded by the Ministry of Education (2017R1A6A1A03015876, 2021R1A6A3A01086488). This research was supported by a Korea Basic Science Institute (National Research Facilities and Equipment Center) grant funded by the Ministry of Education (grant No. 2021R1A6C101C369).

Availability of data and materials
The data that support the findings of this study are available within the article and the Supplementary Information. All other raw data are available upon reasonable request from the corresponding author.

Declarations

Ethics approval and consent to participate
The animal experiments in this study were approved by the Jeonbuk National University Animal Care and Use Committee. Ethical approval was obtained from the ethics committee of Jeonbuk National University (Project title: Development of new therapeutic candidates for prion disease and discovery of early diagnosis biomarkers; Approval no. JBNU 2020–080; Date of approval: 2020–06-25).

Consent for publication
Not applicable.

Competing interest
The authors declare that they have no competing interests.

Author details
[1]Korea Zoonosis Research Institute, Jeonbuk National University, Iksan 54531, Republic of Korea. [2]Department of Bioactive Material Sciences and Institute for Molecular Biology and Genetics, Jeonbuk National University, Jeonju 54896, Republic of Korea. [3]Department of Surgery, College of Veterinary Medicine, South Valley University, Qena 83523, Egypt. [4]Department of Biological Sciences, Andong National University, Andong 36729, Republic of Korea. [5]School of Life Sciences and Biotechnology, Gyeongkuk National University, Andong 36729, Republic of Korea.

Received: 22 March 2024 Accepted: 11 March 2025
Published online: 28 March 2025

References

1. Prusiner SB. The prion diseases. Brain Pathol. 1998;8(3):499–513. https://doi.org/10.1111/j.1750-3639.1998.tb00171.x.
2. Shen L, Ji H-F. Conformational conversion and prion disease. Nat Rev Mol Cell Biol. 2011;12(4):273–273. https://doi.org/10.1038/nrm3007-c1.
3. Sigurdson CJ, Bartz JC, Glatzel M. Cellular and molecular mechanisms of prion disease. Annu Rev Pathol. 2019;14:497–516. https://doi.org/10.1146/annurev-pathmechdis-012418-013109.
4. Aguzzi A, Heikenwalder M, Polymenidou M. Insights into prion strains and neurotoxicity. Nat Rev Mol Cell Biol. 2007;8(7):552–61. https://doi.org/10.1038/nrm2204.
5. Soto C, Satani N. The intricate mechanisms of neurodegeneration in prion diseases. Trends Mol Med. 2011;17(1):14–24. https://doi.org/10.1016/j.molmed.2010.09.001.
6. Ligios C, Cancedda GM, Margalith I, Santucciu C, Madau L, Maestrale C, Basagni M, Saba M, Heikenwalder M. Intraepithelial and interstitial deposition of pathological prion protein in kidneys of scrapie-affected sheep. PLoS ONE. 2007;2(9): e859. https://doi.org/10.1371/journal.pone.0000859.
7. Satoh K, Fuse T, Nonaka T, et al. Postmortem quantitative analysis of prion seeding activity in the digestive system. Molecules. 2019. https://doi.org/10.3390/molecules24244601.
8. Douet JY, Lacroux C, Aron N, et al. Distribution and quantitative estimates of variant creutzfeldt-jakob disease prions in tissues of clinical and asymptomatic patients. Emerg Infect Dis. 2017;23(6):946–56. https://doi.org/10.3201/eid2306.161734.
9. Race B, Meade-White K, Oldstone MB, Race R, Chesebro B. Detection of prion infectivity in fat tissues of scrapie-infected mice. PLoS Pathog. 2008;4(12): e1000232. https://doi.org/10.1371/journal.ppat.1000232.
10. Ding DC, Shyu WC, Lin SZ. Mesenchymal stem cells. Cell Transplant. 2011;20(1):5–14. https://doi.org/10.3727/096368910x.
11. Pittenger MF, Discher DE, Péault BM, Phinney DG, Hare JM, Caplan AI. Mesenchymal stem cell perspective: cell biology to clinical progress. npj Regen Med. 2019;4(1):22. https://doi.org/10.1038/s41536-019-0083-6.
12. Zayed M, Caniglia C, Misk N, Dhar MS. Donor-matched comparison of chondrogenic potential of equine bone marrow- and synovial fluid-derived mesenchymal stem cells: implications for cartilage tissue regeneration. Front Vet Sci. 2016;3:121. https://doi.org/10.3389/fvets.2016.00121.
13. Li M, Chen H, Zhu M. Mesenchymal stem cells for regenerative medicine in central nervous system. Front Neurosci. 2022;16:1068114. https://doi.org/10.3389/fnins.2022.1068114.
14. Fu X, Liu G, Halim A, Ju Y, Luo Q, Song AG. Mesenchymal stem cell migration and tissue repair. Cells. 2019. https://doi.org/10.3390/cells8080784.
15. Zayed M, Kook SH, Jeong BH. Potential therapeutic use of stem cells for prion diseases. Cells. 2023. https://doi.org/10.3390/cells12192413.
16. Lee HC, An SG, Lee HW, et al. Safety and effect of adipose tissue-derived stem cell implantation in patients with critical limb ischemia: a pilot study. Circ J. 2012;76(7):1750–60. https://doi.org/10.1253/circj.cj-11-1135.
17. Al-Ghadban S, Artiles M, Bunnell BA. Adipose stem cells in regenerative medicine: looking forward. Front Bioeng Biotech. 2022. https://doi.org/10.3389/fbioe.2021.837464.
18. Zhang J, Liu Y, Chen Y, Yuan L, Liu H, Wang J, Liu Q, Zhang Y. Adipose-derived stem cells: current applications and future directions in the regeneration of multiple tissues. Stem Cells Int. 2020;2020:8810813. https://doi.org/10.1155/2020/8810813.
19. Yildirim S, Oylumlu E, Ozkan A, Sinen O, Bulbul M, Goksu ET, Ertosun MG, Tanriover G. Zinc (Zn) and adipose-derived mesenchymal stem cells (AD-MSCs) on MPTP-induced Parkinson's disease model: a comparative evaluation of behavioral and immunohistochemical results. Neurotoxicology. 2023;97:1–11. https://doi.org/10.1016/j.neuro.2023.05.002.
20. Hay AJD, Latham AS, Mumford G, et al. Intranasally delivered mesenchymal stromal cells decrease glial inflammation early in prion disease. Front Neurosci. 2023;17:1158408. https://doi.org/10.3389/fnins.2023.1158408.
21. Zayed M, Jeong BH. Adipose-derived mesenchymal stem cell secretome attenuates prion protein peptide (106–126)-induced oxidative stress via Nrf2 activation. Stem Cell Rev Rep. 2024. https://doi.org/10.1007/s12015-024-10811-6.
22. Fast C, Keller M, Kaatz M, Ziegler U, Groschup MH. Low levels of classical BSE infectivity in rendered fat tissue. Vet Res. 2018;49(1):122. https://doi.org/10.1186/s13567-018-0618-7.
23. Lyahyai J, Mediano DR, Ranera B, Sanz A, Remacha AR, Bolea R, Zaragoza P, Rodellar C, Martín-Burriel I. Isolation and characterization of ovine mesenchymal stem cells derived from peripheral blood. BMC Vet Res. 2012;8(1):169. https://doi.org/10.1186/1746-6148-8-169.
24. Hernaiz A, Cobeta P, Marín B, Vázquez FJ, Badiola JJ, Zaragoza P, Bolea R, Martín-Burriel I. Susceptibility of ovine bone marrow-derived mesenchymal stem cell spheroids to scrapie prion infection. Animals (Basel). 2023. https://doi.org/10.3390/ani13061043.
25. Cervenakova L, Akimov S, Vasilyeva I, Yakovleva O, McKenzie C, Cervenak J, Piccardo P, Asher DM. Fukuoka-1 strain of transmissible spongiform encephalopathy agent infects murine bone marrow-derived cells with features of mesenchymal stem cells. Transfusion. 2011;51(8):1755–68. https://doi.org/10.1111/j.1537-2995.2010.03041.x.
26. Takakura Y, Yamaguchi N, Nakagaki T, Satoh K, Kira J-I, Nishida N. Bone marrow stroma cells are susceptible to prion infection. Biochem Biophys Res Commun. 2008;377(3):957–61. https://doi.org/10.1016/j.bbrc.2008.10.099.
27. Patel GD, Liu L, Li A, Yang Y-H, Shen C-C, Brand-Saberi B, Yang X. Mesenchymal stem cell-based therapies for treating well-studied neurological disorders: a systematic review. Front Med. 2024. https://doi.org/10.3389/fmed.2024.1361723.
28. Varghese J, Griffin M, Mosahebi A, Butler P. Systematic review of patient factors affecting adipose stem cell viability and function: implications for

regenerative therapy. Stem Cell Res Ther. 2017;8(1):45. https://doi.org/10.1186/s13287-017-0483-8.
29. Zayed M, Adair S, Ursini T, Schumacher J, Misk N, Dhar M. Concepts and challenges in the use of mesenchymal stem cells as a treatment for cartilage damage in the horse. Res Vet Sci. 2018;118:317–23. https://doi.org/10.1016/j.rvsc.2018.03.011.
30. Li C, Zhao H, Cheng L, Wang B. Allogeneic vs. autologous mesenchymal stem/stromal cells in their medication practice. Cell Biosci. 2021;11(1):187. https://doi.org/10.1186/s13578-021-00698-y.
31. Efimenko AY, Kochegura TN, Akopyan ZA, Parfyonova YV. Autologous stem cell therapy: how aging and chronic diseases affect stem and progenitor cells. Biores Open Access. 2015;4(1):26–38. https://doi.org/10.1089/biores.2014.0042.
32. Shin L, Peterson DA. Impaired therapeutic capacity of autologous stem cells in a model of type 2 diabetes. Stem Cells Transl Med. 2012;1(2):125–35. https://doi.org/10.5966/sctm.2012-0031.
33. Tan L, Liu X, Dou H, Hou Y. Characteristics and regulation of mesenchymal stem cell plasticity by the microenvironment - specific factors involved in the regulation of MSC plasticity. Genes Dis. 2022;9(2):296–309. https://doi.org/10.1016/j.gendis.2020.10.006.
34. Metzker ML. Sequencing technologies - the next generation. Nat Rev Genet. 2010;11(1):31–46. https://doi.org/10.1038/nrg2626.
35. Kim Y-C, Won S-Y, Jeong B-H. Altered expression of glymphatic system-related proteins in prion diseases: Implications for the role of the glymphatic system in prion diseases. Cell Mol Immunol. 2021;18(9):2281–3. https://doi.org/10.1038/s41423-021-00747-z.
36. Iohara K, Zayed M, Takei Y, Watanabe H, Nakashima M. Treatment of pulpectomized teeth with trypsin prior to transplantation of mobilized dental pulp stem cells enhances pulp regeneration in aged dogs. Front Bioeng Biotechnol. 2020;8:983. https://doi.org/10.3389/fbioe.2020.00983.
37. Zayed M, Iohara K, Watanabe H, Ishikawa M, Tominaga M, Nakashima M. Characterization of stable hypoxia-preconditioned dental pulp stem cells compared with mobilized dental pulp stem cells for application for pulp regenerative therapy. Stem Cell Res Ther. 2021;12(1):302. https://doi.org/10.1186/s13287-021-02240-w.
38. Zomer HD, Varela GKds, Delben PB, Heck D, Jeremias T, Trentin AG. In vitro comparative study of human mesenchymal stromal cells from dermis and adipose tissue for application in skin wound healing. J Tissue Eng Regen Med. 2019;13(5):729–41. https://doi.org/10.1002/term.2820.
39. Sim H-J, Kim Y-C, Bhattarai G, Won S-Y, Lee J-C, Jeong B-H, Kook S-H. Prion infection modulates hematopoietic stem/progenitor cell fate through cell-autonomous and non-autonomous mechanisms. Leukemia. 2023;37(4):877–87. https://doi.org/10.1038/s41375-023-01828-w.
40. Vanni I, Iacobone F, D'Agostino C, et al. An optimized Western blot assay provides a comprehensive assessment of the physiological endoproteolytic processing of the prion protein. J Biol Chem. 2023;299(2): 102823. https://doi.org/10.1016/j.jbc.2022.102823.
41. Carroll JA, Striebel JF, Rangel A, Woods T, Phillips K, Peterson KE, Race B, Chesebro B. Prion strain differences in accumulation of PrPSc on neurons and glia are associated with similar expression profiles of neuroinflammatory genes: comparison of three prion strains. PLoS Pathog. 2016;12(4): e1005551. https://doi.org/10.1371/journal.ppat.1005551.
42. Dominici M, Le Blanc K, Mueller I, et al. Minimal criteria for defining multipotent mesenchymal stromal cells. the International society for cellular therapy position statement. Cytotherapy. 2006;8(4):315–7. https://doi.org/10.1080/14653240600855905.
43. Anderson P, Carrillo-Gálvez AB, García-Pérez A, Cobo M, Martín F. CD105 (endoglin)-negative murine mesenchymal stromal cells define a new multipotent subpopulation with distinct differentiation and immunomodulatory capacities. PLoS ONE. 2013;8(10): e76979. https://doi.org/10.1371/journal.pone.0076979.
44. Li J, Deng T, Zhu S, Xie P, Wang W, Zhou H, Xu C. The SDF-1/CXCR4 axis is involved in adipose-derived stem cell migration. Neurourol Urodyn. 2024;43(8):2279–89. https://doi.org/10.1002/nau.25571.
45. Liddelow SA, Guttenplan KA, Clarke LE, et al. Neurotoxic reactive astrocytes are induced by activated microglia. Nature. 2017;541(7638):481–7. https://doi.org/10.1038/nature21029.
46. Kim T-K, Lee I, Cho J-H, Canine B, Keller A, Price ND, Hwang D, Carlson G, Hood L. Core transcriptional regulatory circuits in prion diseases. Mol Brain. 2020;13(1):10. https://doi.org/10.1186/s13041-020-0551-3.
47. Assis-de-Lemos G, Moura-do-Nascimento R, Amaral-do-Nascimento M, Miceli AC, Vieira TCRG. Vieira interactions between cytokines and the pathogenesis of prion diseases: insights and implications. Brain Sci. 2024. https://doi.org/10.3390/brainsci14050413.
48. Hernandez A, Stohn JP. The type 3 deiodinase: epigenetic control of brain thyroid hormone action and neurological function. Int J Mol Sci. 2018. https://doi.org/10.3390/ijms19061804.
49. Carroll JA, Striebel JF, Race B, Phillips K, Chesebro B. Prion infection of mouse brain reveals multiple new upregulated genes involved in neuroinflammation or signal transduction. J Virol. 2015;89(4):2388–404. https://doi.org/10.1128/jvi.02952-14.
50. Li JY, Paragas N, Ned RM, et al. Scara5 is a ferritin receptor mediating non-transferrin iron delivery. Dev Cell. 2009;16(1):35–46. https://doi.org/10.1016/j.devcel.2008.12.002.
51. Ganz T, Nemeth E. Hepcidin and iron homeostasis. Biochim et Biophys Acta (BBA) - Molecular Cell Res. 2012;1823(9):1434–43. https://doi.org/10.1016/j.bbamcr.2012.01.014.
52. Singh A, Isaac AO, Luo X, Mohan ML, Cohen ML, Chen F, Kong Q, Bartz J, Singh N. Abnormal brain iron homeostasis in human and animal prion disorders. PLoS Pathog. 2009;5(3): e1000336. https://doi.org/10.1371/journal.ppat.1000336.
53. Singh N, Haldar S, Tripathi AK, McElwee MK, Horback K, Beserra A. Iron in neurodegenerative disorders of protein misfolding: a case of prion disorders and Parkinson's disease. Antioxid Redox Signal. 2014;21(3):471–84. https://doi.org/10.1089/ars.2014.5874.
54. Viré EA, Mead S. Gene expression and epigenetic markers of prion diseases. Cell Tissue Res. 2023;392(1):285–94. https://doi.org/10.1007/s00441-022-03603-2.
55. Sivandzade F, Cucullo L. Regenerative stem cell therapy for neurodegenerative diseases: an overview. Int J Mol Sci. 2021. https://doi.org/10.3390/ijms22042153.
56. Krance SH, Luke R, Shenouda M, Israwi AR, Colpitts SJ, Darwish L, Strauss M, Watts JC. Cellular models for discovering prion disease therapeutics: progress and challenges. J Neurochem. 2020;153(2):150–72. https://doi.org/10.1111/jnc.14956.
57. Hickson LJ, Eirin A, Lerman LO. Challenges and opportunities for stem cell therapy in patients with chronic kidney disease. Kidney Int. 2016;89(4):767–78. https://doi.org/10.1016/j.kint.2015.11.023.
58. Zayed M, Iohara K. Effects of p-Cresol on senescence, survival, inflammation, and odontoblast differentiation in canine dental pulp stem cells. Int J Mol Sci. 2020. https://doi.org/10.3390/ijms21186931.
59. Mallam E, Kemp K, Wilkins A, Rice C, Scolding N. Characterization of in vitro expanded bone marrow-derived mesenchymal stem cells from patients with multiple sclerosis. Mult Scler. 2010;16(8):909–18. https://doi.org/10.1177/1352458510371959.
60. Bossolasco P, Cova L, Calzarossa C, Servida F, Mencacci NE, Onida F, Polli E, Lambertenghi Deliliers G, Silani V. Metalloproteinase alterations in the bone marrow of ALS patients. J Mol Med (Berl). 2010;88(6):553–64. https://doi.org/10.1007/s00109-009-0584-7.
61. Hetz C, Russelakis-Carneiro M, Maundrell K, Castilla J, Soto C. Caspase-12 and endoplasmic reticulum stress mediate neurotoxicity of pathological prion protein. Embo j. 2003;22(20):5435–45. https://doi.org/10.1093/emboj/cdg537.
62. Song CH, Honmou O, Furuoka H, Horiuchi M. Identification of chemoattractive factors involved in the migration of bone marrow-derived mesenchymal stem cells to brain lesions caused by prions. J Virol. 2011;85(21):11069–78. https://doi.org/10.1128/jvi.05318-11.
63. Miller RJ, Banisadr G, Bhattacharyya BJ. CXCR4 signaling in the regulation of stem cell migration and development. J Neuroimmunol. 2008;198(1–2):31–8. https://doi.org/10.1016/j.jneuroim.2008.04.008.
64. Lapidot T. Mechanism of human stem cell migration and repopulation of NOD/SCID and B2mnull NOD/SCID mice. the role of SDF-1/CXCR4 interactions. Ann N Y Acad Sci. 2001;938:83–95. https://doi.org/10.1111/j.1749-6632.2001.tb03577.x.
65. Hong S, Beja-Glasser VF, Nfonoyim BM, et al. Complement and microglia mediate early synapse loss in alzheimer mouse models. Science. 2016;352(6286):712–6. https://doi.org/10.1126/science.aad8373.
66. Wang T-T, Tian C, Sun J, et al. Down-regulation of brain-derived neurotrophic factor and its signaling components in the brain tissues of scrapie experimental animals. Int J Biochem Cell Biol. 2016;79:318–26. https://doi.org/10.1016/j.biocel.2016.08.033.

67. López González I, Garcia-Esparcia P, Llorens F, Ferrer I. Genetic and transcriptomic profiles of inflammation in neurodegenerative diseases: alzheimer, parkinson, creutzfeldt-jakob and tauopathies. Int J Mol Sci. 2016;17(2):206. https://doi.org/10.3390/ijms17020206.
68. Richardson EP Jr, Masters CL. The nosology of Creutzfeldt-Jakob disease and conditions related to the accumulation of PrPCJD in the nervous system. Brain Pathol. 1995;5(1):33–41. https://doi.org/10.1111/j.1750-3639.1995.tb00575.x.
69. Imberdis T, Harris DA. Prion permissive pathways: extracellular matrix genes control susceptibility to prion infection. Embo j. 2014;33(14):1506–8. https://doi.org/10.15252/embj.201489071.
70. Filali H, Martin-Burriel I, Harders F, et al. Gene expression profiling and association with prion-related lesions in the medulla oblongata of symptomatic natural scrapie animals. PLoS ONE. 2011;6(5): e19909. https://doi.org/10.1371/journal.pone.0019909.
71. Mohan H, Krumbholz M, Sharma R, et al. Extracellular matrix in multiple sclerosis lesions: fibrillar collagens, biglycan and decorin are upregulated and associated with infiltrating immune cells. Brain Pathol. 2010;20(5):966–75. https://doi.org/10.1111/j.1750-3639.2010.00399.x.
72. Tong Y, Xu Y, Scearce-Levie K, Ptácek LJ, Fu YH. COL25A1 triggers and promotes Alzheimer's disease-like pathology in vivo. Neurogenetics. 2010;11(1):41–52. https://doi.org/10.1007/s10048-009-0201-5.
73. Bradford BM, Mabbott NA. Prion disease and the innate immune system. Viruses. 2012;4(12):3389–419. https://doi.org/10.3390/v4123389.
74. Aguzzi A, Heikenwalder M. Prions, cytokines, and chemokines: a meeting in lymphoid organs. Immunity. 2005;22(2):145–54. https://doi.org/10.1016/j.immuni.2004.12.007.
75. Mabbott NA, Alibhai JD, Manson J. The role of the immune system in prion infection. In: Human Prion Diseases. Elsevier; 2018. p. 85–107. https://doi.org/10.1016/B978-0-444-63945-5.00005-2.
76. Li B, Chen M, Zhu C. Neuroinflammation in prion disease. Int J Mol Sci. 2021. https://doi.org/10.3390/ijms22042196.
77. Lin CF, Yu KH, Jheng CP, Chung R, Lee CI. Curcumin reduces amyloid fibrillation of prion protein and decreases reactive oxidative stress. Pathogens. 2013;2(3):506–19. https://doi.org/10.3390/pathogens2030506.
78. Tabaee Damavandi P, Dove MT, Pickersgill RW. A review of drug therapy for sporadic fatal insomnia. Prion. 2017;11(5):293–9. https://doi.org/10.1080/19336896.2017.1368937.
79. Joo M, Sadikot RT. PGD synthase and PGD2 in immune resposne. Mediators Inflamm. 2012;2012: 503128. https://doi.org/10.1155/2012/503128.
80. Tribouillard-Tanvier D, Race B, Striebel JF, Carroll JA, Phillips K, Chesebro B. Early cytokine elevation, PrPres deposition, and gliosis in mouse scrapie: no effect on disease by deletion of cytokine genes IL-12p40 and IL-12p35. J Virol. 2012;86(19):10377–83. https://doi.org/10.1128/jvi.01340-12.
81. He P, Zhong Z, Lindholm K, Berning L, Lee W, Lemere C, Staufenbiel M, Li R, Shen Y. Deletion of tumor necrosis factor death receptor inhibits amyloid beta generation and prevents learning and memory deficits in Alzheimer's mice. J Cell Biol. 2007;178(5):829–41. https://doi.org/10.1083/jcb.200705042.
82. Shan Z, Hirai Y, Nakayama M, Hayashi R, Yamasaki T, Hasebe R, Song CH, Horiuchi M. Therapeutic effect of autologous compact bone-derived mesenchymal stem cell transplantation on prion disease. J Gen Virol. 2017;98(10):2615–27. https://doi.org/10.1099/jgv.0.000907.
83. Chaudhary S, Ashok A, Wise AS, Rana NA, McDonald D, Kritikos AE, Kong Q, Singh N. Upregulation of brain hepcidin in prion diseases. Prion. 2021;15(1):126–37. https://doi.org/10.1080/19336896.2021.1946377.
84. Stepanić V, Kučerová-Chlupáčová M. Review and chemoinformatic analysis of ferroptosis modulators with a focus on natural plant products. Molecules. 2023. https://doi.org/10.3390/molecules28020475.
85. Massaiu I, Campodonico J, Mapelli M, et al. Dysregulation of iron metabolism-linked genes at myocardial tissue and cell levels in dilated cardiomyopathy. Int J Mol Sci. 2023. https://doi.org/10.3390/ijms24032887.
86. Kong W-N, Gao G, Chang Y-Z. Hepcidin and sports anemia. Cell Biosci. 2014;4(1):19. https://doi.org/10.1186/2045-3701-4-19.
87. Majerníková NA, den Dunnen WFA, Dolga AM. The potential of ferroptosis-targeting therapies for alzheimer's disease: from mechanism to transcriptomic analysis. Front Aging Neurosci. 2021. https://doi.org/10.3389/fnagi.2021.745046.

Publisher's Note